

# On-chip Light Trapping in Bilayer Moiré Photonic Crystal Slabs

Haoning Tang<sup>1</sup>⊥, Xueqi Ni<sup>1</sup>⊥, Fan Du<sup>1</sup>, Eric Mazur<sup>1</sup>\*

<sup>1</sup>School of Engineering and Applied Sciences, Harvard University, Cambridge, MA 02138, USA

⊥ Authors contributed equally to this work

\* Email: [mazur@seas.harvard.edu](mailto:mazur@seas.harvard.edu)

## Abstract

There has been remarkable recent progress in the formation of nano-resonators that support ultra-low-loss, compact dielectric photonic crystals with exceptional high-Q modes that operate at visible or telecom wavelength [1-3]. New insights into “modal engineering” have recently emerged from researchers exploring exotic electronic phases in so-called “2D materials” [4, 5]. The phenomenon relates to a twist in the angle between two layers of materials with high periodic spatial ordering, such as graphene. A moiré pattern forms, and at a particular magic-angle of twist, the electronic behavior significantly changes, enjoying a flat energy-momentum dispersion relationship. There is an optical analog to the electron twistrionics: bilayer moiré photonic crystal slabs can realize a flat-band condition [6, 7]. Under these conditions, the propagating modes have zero group velocity, thus giving rise to momentum-free trapping of Bloch waves in both transverse and vertical directions, creating high quality-factors (Q-factor  $\sim 10^9$ ) and exceptionally small modal volumes ( $V \sim 5(\lambda/n)^3$ ) that eventually lead to the enhancement of Purcell effect. The dramatically different means of light-localization afforded by moiré-structured cavities, very small mode volumes, and spatial determination by the overall moiré pattern can manipulate spontaneous emission. This provides many opportunities for applications such as low-threshold lasing, single-photon source, quantum electrodynamics, photonic circuit, and quantum information processing [8-12].

## Introduction

Light trapping is a constant pursuit in on-chip photonic devices because of its importance in cavity quantum electrodynamics and nonlinear optics [8, 13-16]. Many mechanisms have been explored, including the photonic crystal cavity that uses defects and photonic crystal band gaps to forbid in-plane propagating waves (Fig. 1 a-b) [17-21]. This results in a highly localized non-Bloch mode; however, there is a detrimental trade-off between the Q-factor and mode volume ( $V$ ) in a cavity, which are determinative values in manipulating the spontaneous emission. Photonic crystal cavities increase the temporal confinement of light in a material, as represented by their increased Q-factor, only by sacrificing modal volume  $V$  because of the non-Bloch mode localization effect (See Fig.1 g) [17]. An alternative approach is to use photonic crystal slabs without defects but provide optical BiCs that do not couple to the external radiation fields at some specific momentum (Fig.1 c-d) [1, 8, 22, 23]. Most BiCs studied in PhC slabs are only localized in the vertical (thickness) direction but remain delocalized in the transverse direction across the slab, rendering them less ideal in enhancing light-matter interaction. Besides, both cavity photonic crystal and BiC photonic crystal are sensitive to fabrication disorders. Therefore, Q factors measured from most BiC experiments turn out to be  $10^4$  to  $10^6$  despite that they should be infinitely large theoretically (Fig.1 g). It is, therefore, of great interest to explore a photonic device that concentrates light in both vertical and transverse directions and is robust to the errors in device fabrication.

Bilayer Moiré photonic crystal slabs provide a desirable balance between Q and V and offer a new means of light localization in materials that address some of the limitations of the more traditionally employed platforms such as defect photonic crystal cavities and photonic crystal slabs (Fig.1 g). Intuitively, Moiré photonic crystals have two sets of periodicities at certain twisted angles: periodicity of the individual photonic lattices and of superlattices [6, 24]. Therefore, the underlying oscillation of the electromagnetic field is comparable to conventional photonic crystals. But the overall profile is also modulated and enveloped by the moiré superlattice periodicity. As a result, the light can be confined in some sites of the superlattice and delocalized in other places (Fig.1 e-f). If we tune the twisted angles of two slabs until the moiré bands become flat, the group velocity of propagating modes drops to zero and generates "stop-light" effects, representing the light-trapping in the transverse direction and narrow bandwidth. Specifically, modes on moiré bands have a high local density of states (LDOS) on the AA stacking site. Besides, vertical confinement of light is achieved since all modes on the moiré bands are high Q mode, making it immune to fabrication errors. As a result, in bilayer moiré photonic crystal slabs, light is confined in the transverse direction due to the moiré pattern of the lateral heterostructure and confined in the vertical direction, providing tunable, momentum-free trapping of Bloch waves in a region that high Q-factors and small V are both accessible. This contrasts with most photonic crystal cavities that have localized non-Bloch modes with small V and relatively low Q-factor, or bound-states-in-continuum photonic crystals with high Q-factors but large V. Bilayer moiré photonic crystals, therefore, are a promising device for better on-chip light trapping and enhancement in spontaneous emission. (Fig.1 g).

In this paper, we present this light-trapping mechanism using the moiré pattern in the bilayer photonic crystal slabs. We numerically demonstrate the Q-factors as high as  $10^9$  and mode volumes  $V \sim 0.8\lambda^2$  in the 1D bilayer photonic crystal gratings, and  $Q \sim 10^8$  and  $V \sim 1.7\lambda^3$  in the 2D bilayer photonic crystal slabs. Bilayer moiré photonic crystals have higher quality factors compared to single-layer moiré photonic crystals [25]. Furthermore, we numerically calculated the plane-wave optical response, LDOS enhancement, and Purcell enhancement in both 1D and 2D bilayer moiré photonic crystals. Our work demonstrates a new method of light trapping that has potential applications in cavity quantum electrodynamics and nonlinear optics.

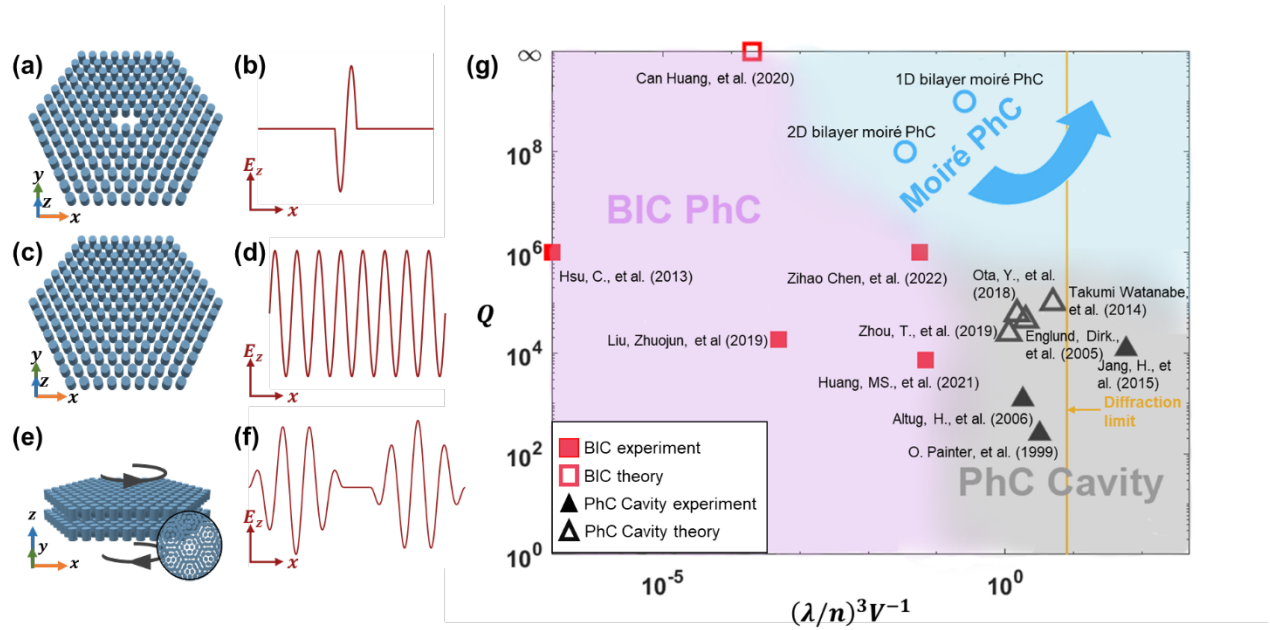


Figure 1 Photonic crystal structures and their electromagnetic modes. (a) (b) Defect photonic crystal cavity and its in-plane light confinement; (c) (d) High Q 2D photonic crystal slabs with guided Bloch modes, such as the bound-states-in-continuum photonic crystals; (e) (f) Twisted bilayer moiré photonic crystal. The amplitude of the electromagnetic field is modulated by the moiré superlattice. (g) Comparison of Q-factor and mode volume for photonic crystal cavity, BiC photonic crystals, and moiré photonic crystals.

## Results and Discussion

**Band structure and Q-factors.** We studied both 1D moiré photonic crystal slabs and 2D moiré photonic crystal slabs. 1D moiré photonic crystal slabs have periodicity along with one of its in-plane axis and finite height along the out-of-plane axis, while the 2D moiré photonic crystal slabs have periodicity along with two of its in-plane axis and finite height along the out-of-plane axis. Both 1D and 2D bilayer moiré photonic crystal slabs have all-momentum high-Q flat bands, but the two systems have different types of optical responses, given the variation in the complexity of Bloch waves vectors.

The first system consists of two 1D photonic crystal slabs that are subwavelength high refractive index contrast gratings but with different periodicity [7]. These gratings have the same thickness  $h = 180 \text{ nm}$  and filling fraction  $\kappa = 0.8$  and are separated by only a subwavelength distance  $L = 0.1185a$ , where  $a = 300 \text{ nm}$  is the base lattice constant. The periods of gratings are slightly different but satisfy the commensurate condition  $\frac{a_1}{a_2} = N/(N + 1)$  for a natural number  $N$  (see fig. 2a), and  $a_1 = \frac{2N}{2N+1}a$ . The shift behavior produces a moiré pattern with a macroscopic periodicity of distinct AA (mostly aligned) and AB/BA (mostly misaligned) stacking regions that grow in size as  $N$  increases. The moiré band structure is calculated using the finite-element method (see fig. 2b). Two isolated bands with small slopes appear in the bandgap, and the flatness of both bands can be tuned simultaneously through the variation of superlattice periodicity, which is represented by  $N$  in this case (see fig. 2b). The flat-band superlattice periodicity is retrieved from the simulation: At the magic superlattice periodicity condition  $N = 19$ , two completely flat-bands appear in the bandgap and the flatness is optimized, indicating the highest density-of-states (see fig. 2c). Flat-band states would give rise to an unconventional light-trapping regime: Bonding light-trapping mode at a higher frequency and antibonding light-trapping mode at a lower frequency. The Q-factor of moiré modes on all k-vectors is as high as  $10^9$ , indicating the all-momentum flat-band light-trapping in the vertical direction.

The second system is the twisted bilayer photonic crystals (TBPhCs) that are built by twisting two identical honeycomb lattices against each other (see fig. 2d)[6]. The 2D photonic crystal is a  $d = 220 \text{ nm}$  thick crystalline silicon membrane ( $n_{Si} = 3.48$ ) with  $C_{6v}$  symmetry-protected triangular shape air holes. The triangular holes have a side length of  $b = 279 \text{ nm}$ , and the unit cell pitch is  $a = 478 \text{ nm}$ . The interlayer tunneling membrane has a thickness of  $h = 250 \text{ nm}$ , and a refractive index of polymethyl methacrylate (PMMA)  $n_{PMMA} = 1.48$ . The twist behavior also produces a moiré pattern with distinct AA (mostly aligned) and AB/BA (mostly misaligned) stacking regions that grow in size as the twisted angle decreases. The superlattice is formed by the lattice of two layers of photonic crystals and results in a smaller Brillouin zone. The rotation between two layers causes two sets of Dirac cones to intersect and hybridize with each other. It also causes the guided resonances in the two twisted PhC layers to couple through an evanescent tunneling pathway which is stronger in the AA site than the AB/BA site. As the angle gets smaller and smaller, the Dirac-cone bands hybridize with each other, and the tunneling of electromagnetic modes between the two layers increases. The flattening of the bands near the magic angle can be understood as compensation between the kinetic energy and the interlayer hybridization energy (see Fig. 2e). As the twist angle gets smaller, the Dirac cone bands get closer to each other, and they hybridize into the flattest bands at the ‘magic twist angle’ ( $\theta = 1.89^\circ$ ). In our previous published work, we present TBPhCs with ultra-flat photonic bands that exhibit extreme slow light behavior in the C-band of the telecom window. And the flat band at  $\theta = 1.89^\circ$  has an ultra-narrow bandwidth of 0.217 THz and vanishing group velocity. The Q-factors of all moiré flat-band modes are approximately  $10^8$ , which indicates the light is highly trapped in the vertical direction without radiative loss into the far-field. The precision of the mesh of our simulation is limited by the computation resources, as a result, the real Q-factor is expected to be even higher than the result demonstrated in this paper.

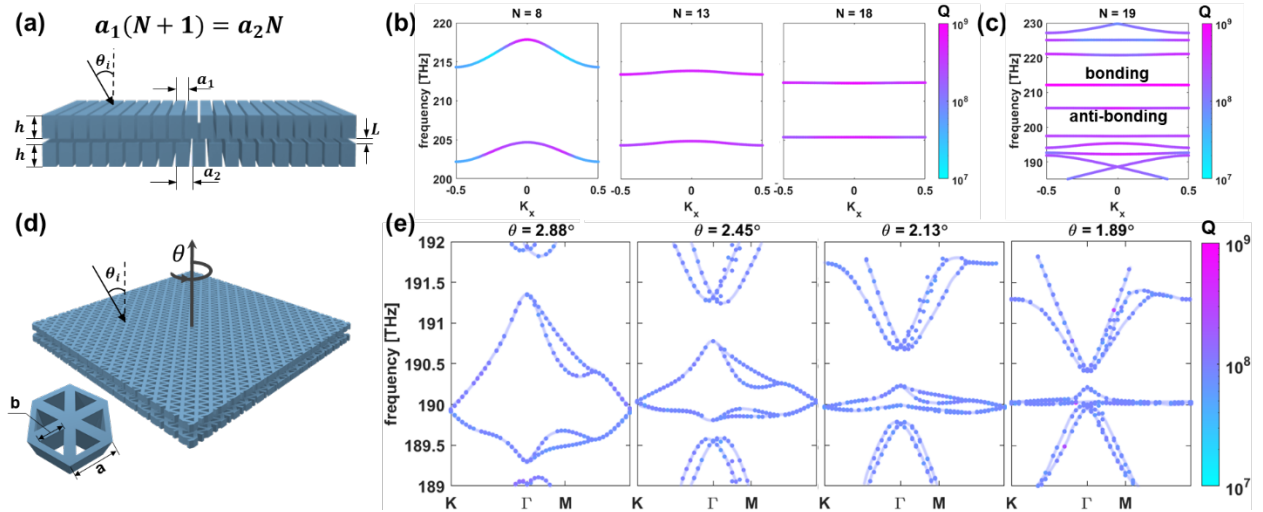


Figure 2 Band evolutions and Q factors. (a) The geometry of 1D moiré grating under commensurate conditions; (b) Band structure and its evolution with respect to the number of arrays in a superlattice,  $N$ . Color bar indicates Q-factor; (c) Zoomed-out band diagram and two optimized flat bands related to bonding and anti-bonding modes; (d) Geometry of 2D twisted bilayer photonic crystals. (e) Band structure evolution as a function of twisted angle  $\theta$ , showing the hybridization of Dirac cones and appearance of flat-band at around 190THz. The color bar also indicates the Q-factor.

**Optical response and mode volume.** We then studied the optical responses of the 1D and 2D bilayer moiré photonic crystals slabs and further explored the transverse light-trapping through the mode volume. In the 1D moiré photonic crystals, the resonances in transmission and reflection curves show the robustness to the incident angle  $\theta_i$  because of the existence of the flat bands (Fig.3 a). At the resonance frequency, both the bonding band and the antibonding band are excited by the plane wave

with the incident angle  $\theta_i$  from  $5^\circ$  to  $30^\circ$  (Fig.3 b). The mode volume decreases by a factor of 10 at the flat-band modes and is insensitive to the incident angle (Fig.3 c). In the 2D moiré photonic crystals, no far-field optical resonances appear under the plane-wave incidences from  $\theta_i = 5^\circ - 30^\circ$ . However, even at the near-field, the moiré flat-band mode was excited, and the electromagnetic modes are therefore trapped as dark mode around the AA site (Fig.3 e). This is because of the existence of various moiré vectors, which is equivalent to adding disorders to the photonic crystal lattice. The mode volume of dark modes also decreases by a factor of 10 at the flat-band mode and is insensitive to the incident angle as a result of the flat-band (Fig.3 f). Therefore, both 1D and 2D bilayer moiré photonic crystals slabs have obvious transverse light-trapping at flat band frequencies.

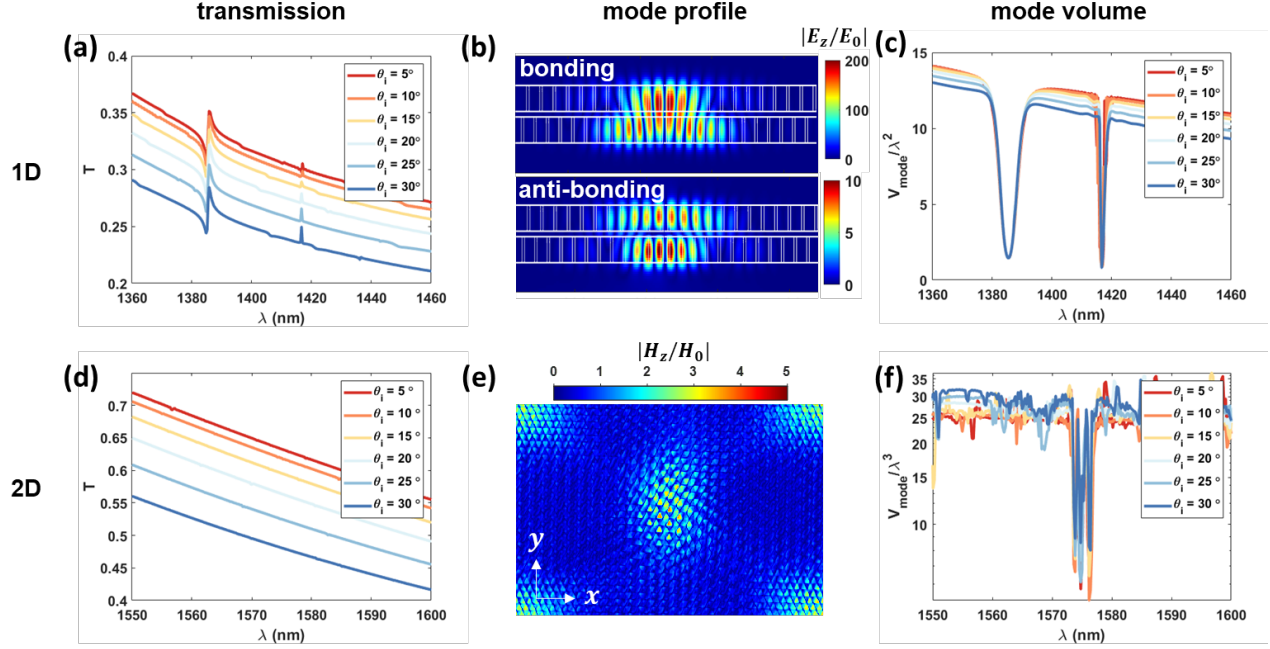


Figure 3 Plane-wave optical responses. (a) Plane-wave incident-angle-resolved transmission spectra of the 1D moiré gratings with  $N = 19$ ; (b) TM mode profiles at bonding and antibonding flat band frequencies, which have been normalized to the electric field of the source,  $E_0$ ; (c) Mode volume spectra with different incident angles at  $N = 19$  (See supplementary material for calculation details); (d) Incident angle-resolved transmission spectra of the 2D moiré slabs with dark resonance. (e) TE mode profile at flat-band frequency, showing light trapping at AA stacking region. The mode amplitude is normalized to the magnetic field of the source,  $H_0$ ; (f) Incident angle-resolved mode volume of the 2D twisted bilayer photonic crystals with twist angle  $\theta = 2.13^\circ$ .

**LDOS and Purcell enhancement.** While the bilayer moiré photonic crystals slabs would give rise to a light-trapping regime in both vertical and transverse direction, it also leads to the enhancement of the local-density-of-states (LDOS) and therefore the Purcell effect. We calculated the LDOS of 1D and 2D moiré photonic crystals by putting a dipole point source in the structure[26, 27]. The dyadic Green's function  $\mathbf{G}$  is defined by the electric field at the point  $r$ , generated by a point source at point  $r_0$  with dipole moment  $\mu$ ,

$$\mathbf{E}(\mathbf{r}) = \frac{\omega^2}{\epsilon_0 \epsilon_r c^2} \mathbf{G}(\mathbf{r}, \mathbf{r}_0) \cdot \boldsymbol{\mu} \quad (1.)$$

where  $\mathbf{G}$  is a  $3 \times 3$  symmetric matrix, therefore each component of  $\mathbf{G}$  can be calculated using the corresponding dipole orientation and electric field component. In both 1D and 2D photonic structures,

we only consider TM-like modes or TE-like modes, which can be represented by  $E_z$  or  $H_z$  in the  $z$ -direction. The dyadic Green's function at  $z$ -direction ( $\mathbf{G}_{zz}$ ) can be calculated from a dipole oriented along the  $z$ -direction as

$$\mathbf{G}_{zz} = \frac{\varepsilon_0 \varepsilon_r c^2 \omega^2}{\mu \omega^2} E_z \quad (2.)$$

The partial local density of states along one direction say  $z$ , can then be obtained from the imaginary part of the dyadic Green's function,

$$\rho_z(r_0, \omega) = \frac{6\omega}{\pi c^2} [Im G_{zz}(r, r_0, \omega)] \quad (3.)$$

Our simulation results first indicate spatial enhancement of the LDOS at the flat-band frequency: In the 1D moiré photonic crystal, the LDOS at the flat bands is enhanced by a factor of 293 for the anti-bonding band  $f = 207.6\text{THz}$  and 838 for the bonding band  $f = 216.2\text{THz}$  at the AA-stacked region compared to the AB-stacked region (Fig.4 a-b). The anti-bonding band has a higher value of LDOS at the AA region due to the higher transverse mode concentration compared to the bonding band. In the 2D moiré photonic crystal, two sets of Dirac-cone bands hybridize to flat bands, thus there is LDOS enhancement at two frequencies:  $190.3\text{THz}$  and  $190.2\text{THz}$ . The LDOS at the AA-stacked region of the moiré flat band is enhanced approximately three orders compared to the AB-stacked region.

The LDOS enhancement leads to an increase in the single-atom decay rate relative to free space, i.e. Purcell enhancement [28], which is crucial for enhancing spontaneous emission. The Purcell factor is calculated by the ratio of the single-atom decay rate in the material over the decay rate in the vacuum, which is also proportional to the LDOS in the material as well. Having all the other constants of materials canceled out, the Purcell factor is reduced to,

$$PF = \frac{Im[\mathbf{G}(\mathbf{r}_i, \mathbf{r}_j, \omega_j)]}{Im[\mathbf{G}_0(\mathbf{r}_i, \mathbf{r}_j, \omega_j)]} \quad (4.)$$

where  $\mathbf{G}(\mathbf{r}_i, \mathbf{r}_j, \omega_j)$  is the dyadic Green's function of point source in the photonic crystal slabs, and  $\mathbf{G}_0(\mathbf{r}_i, \mathbf{r}_j, \omega_j)$  is dyadic Green's function of point source in the free space. Our result shows both 1D and 2D moiré photonic crystal slabs have Purcell enhancement at the flat-band frequencies. In the 1D bilayer moiré photonic crystal slabs, the Purcell enhancement is  $PF = 25$  at  $f = 207.6\text{THz}$  and  $PF = 285$  at band  $f = 216.2\text{THz}$ . In the 2D and bilayer moiré photonic crystal slabs, the Purcell enhancement is  $PF = 109$  at band  $f = 190.2\text{THz}$  and  $PF = 111$  at band  $f = 190.3\text{THz}$ . The spatial enhancement of LDOS and large Purcell effect at flat band frequencies facilitate the control of spontaneous emission rate. With the bilayer moiré photonic crystals slabs, we can tune the spontaneous emission rates of atoms or molecules simply by changing their frequencies and spatial distributions.

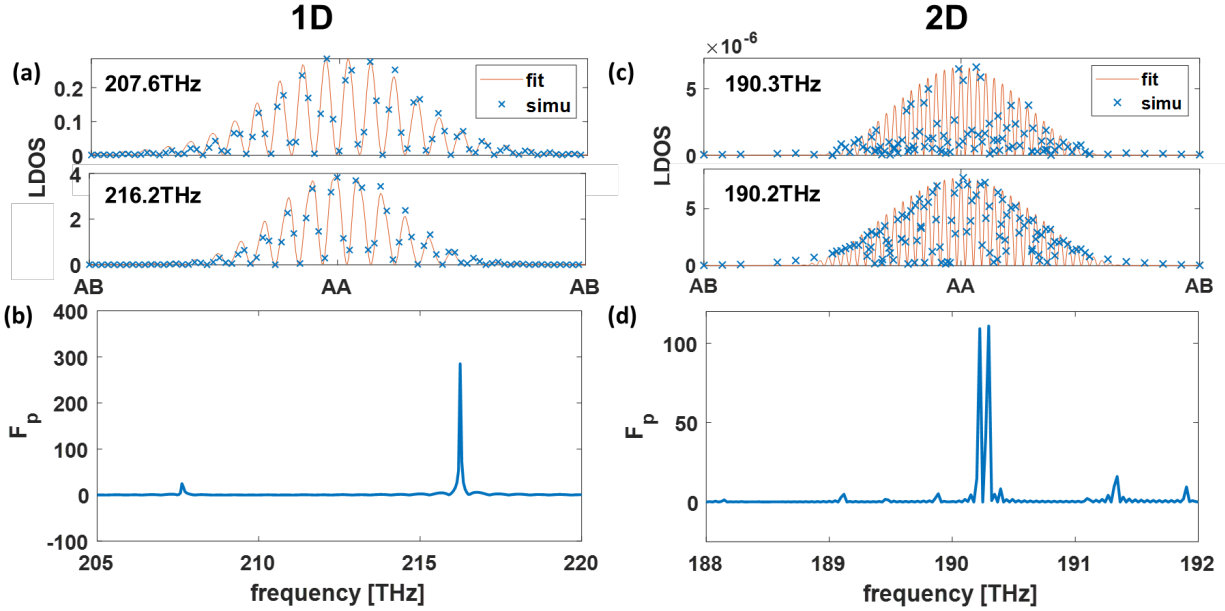


Figure 4 (a) Local density of states in 1D moiré photonic crystal ( $N = 19$ ) at two flat bands and (b) The Purcell factor at different frequencies. (c) Local density of states in 2D twisted bilayer moiré photonic crystal ( $\theta = 2.13^\circ$ ) at two flat bands and (d) the Purcell factor at different frequencies. The simulation result is fitted with a function of  $|\cos(\lambda_1 x)\cos(\lambda_2 x)|^2$ .

## Conclusion

We demonstrated an approach of bilayer moiré photonic crystal slabs to confine light in both transverse and vertical directions, enhancing the LDOS and Purcell effect. Compared to traditional photonic crystal structures such as defect photonic crystal cavity and BIC photonic crystal that have a trade-off between Q and V, bilayer moiré photonic crystals overcome this limitation and allow us to explore a new region where high-Q and small mode volume V can exist simultaneously. We showed that combining high Q and small mode volume enhances spontaneous emission, which is indicated by the spatially enhanced LDOS and Purcell factor in the frequency domain. Notice that besides spatial confinement, the flat band in moiré photonic crystals also concentrate light in frequency domain by narrowing its bandwidth significantly and create slow-light effects, such as higher density-of states and controllable spontaneous emission profile. We believe that the spatial confinement and frequency confinement of the moiré structure together will further create localized light-matter interactions behavior for many other applications such as low-threshold lasing, single-photon source, quantum electrodynamics, photonic circuit, and quantum information processing.

See the supplementary material that outlines in greater detail all the mathematical and simulation methods that we use to calculate the band structure, Q-factor, optical responses, LDOS, and Purcell factors.

Several people contributed to the work described in this paper. H.T. conceived the basic idea for this work. H.T., X.N., and F.D. carried out the simulations and analyzed the results. E.M. supervised the research and the development of the manuscript. X.N. prepared the first draft of the figures. H.T. wrote the first draft of the manuscript; all authors subsequently took part in the revision process and approved the final copy of the manuscript. H.T., X. N., F.D., and E.M. provided feedback on the manuscript throughout its development.

1. Chen, Z., et al., *Observation of miniaturized bound states in the continuum with ultra-high quality factors*. Science Bulletin, 2022. **67**(4): p. 359-366.
2. Jin, J., et al., *Topologically enabled ultrahigh-Q guided resonances robust to out-of-plane scattering*. Nature, 2019. **574**(7779): p. 501-504.
3. Tang, H., et al., *Low-Loss Zero-Index Materials*. Nano Letters, 2021. **21**(2): p. 914-920.
4. Cao, Y., et al., *Correlated insulator behaviour at half-filling in magic-angle graphene superlattices*. Nature, 2018. **556**(7699): p. 80-84.
5. Park, J.M., et al., *Tunable strongly coupled superconductivity in magic-angle twisted trilayer graphene*. Nature, 2021. **590**(7845): p. 249-255.
6. Tang, H., et al., *Modeling the optical properties of twisted bilayer photonic crystals*. Light: Science & Applications, 2021. **10**(1): p. 157.
7. Nguyen, D.X., et al., *Magic configurations in Moiré Superlattice of Bilayer Photonic crystal: Almost-Perfect Flatbands and Unconventional Localization*. arXiv e-prints, 2021: p. arXiv:2104.12774.
8. Kodigala, A., et al., *Lasing action from photonic bound states in continuum*. Nature, 2017. **541**(7636): p. 196-199.
9. Khurgin, J.B. and M.A. Noginov, *How Do the Purcell Factor, the Q-Factor, and the Beta Factor Affect the Laser Threshold?* Laser & Photonics Reviews, 2021. **15**(3): p. 2000250.
10. Vahala, K.J., *Optical microcavities*. Nature, 2003. **424**(6950): p. 839-846.
11. Dahan, R., et al., *Resonant phase-matching between a light wave and a free-electron wavefunction*. Nature Physics, 2020. **16**(11): p. 1123-1131.
12. Yang, Y., et al., *Observation of enhanced free-electron radiation from photonic flatband resonances*. 2021.
13. Hirose, K., et al., *Watt-class high-power, high-beam-quality photonic-crystal lasers*. Nature Photonics, 2014. **8**(5): p. 406-411.
14. Zhou, T., et al., *Continuous-wave quantum dot photonic crystal lasers grown on on-axis Si (001)*. Nature Communications, 2020. **11**(1): p. 977.
15. Watanabe, T., et al., *Array integration of thousands of photonic crystal nanolasers*. Applied Physics Letters, 2014. **104**(12): p. 121108.
16. Jang, H., et al., *Sub-microWatt threshold nanoisland lasers*. Nature Communications, 2015. **6**(1): p. 8276.
17. Joannopoulos, J.D., et al., *Molding the flow of light*. Princeton Univ. Press, Princeton, NJ [ua], 2008.
18. Hu, S. and S.M. Weiss, *Design of Photonic Crystal Cavities for Extreme Light Concentration*. ACS Photonics, 2016. **3**(9): p. 1647-1653.
19. Painter, O., et al., *Two-Dimensional Photonic Band-Gap Defect Mode Laser*. Science, 1999. **284**(5421): p. 1819-1821.
20. Altug, H., D. Englund, and J. Vučković, *Ultrafast photonic crystal nanocavity laser*. Nature Physics, 2006. **2**(7): p. 484-488.
21. Ota, Y., et al., *Topological photonic crystal nanocavity laser*. Communications Physics, 2018. **1**(1).
22. Liu, Z., et al., *High- Q Quasibound States in the Continuum for Nonlinear Metasurfaces*. Physical Review Letters, 2019. **123**(25).
23. Hwang, M.-S., et al., *Ultralow-threshold laser using super-bound states in the continuum*. Nature Communications, 2021. **12**(1).
24. Tang, H., et al. *Twisted Bilayer Dielectric Photonic Crystal Slabs*. in *Conference on Lasers and Electro-Optics*. 2021. San Jose, California: Optica Publishing Group.
25. Mao, X.-R., et al., *Magic-angle lasers in nanostructured moiré superlattice*. Nature Nanotechnology, 2021.

26. Mello, O., et al., *Extended many-body superradiance in diamond epsilon near-zero metamaterials*. Applied Physics Letters, 2022. **120**(6): p. 061105.
27. Mello, O., et al. *Strongly Extended Superradiance in Diamond Metamaterials*. in *Conference on Lasers and Electro-Optics*. 2017. San Jose, California: Optical Society of America.
28. Van Vlack, C.P., *Dyadic green functions and their applications in classical and quantum nanophotonics*. 2012.